A Summary of Convective-Core Vertical Velocity Properties Using ARM UHF Wind Profilers in Oklahoma

SCOTT E. GIANGRANDE,* SCOTT COLLIS,+ JERRY STRAKA,# ALAIN PROTAT,@ CHRISTOPHER WILLIAMS,& AND STEVEN KRUEGER**

* *Atmospheric Sciences Division, Brookhaven National Laboratory, Upton, New York*
+ *Environmental Sciences Division, Argonne National Laboratory, Argonne, Illinois*
# *University of Oklahoma, Norman, Oklahoma*
@ *Bureau of Meteorology, Melbourne, Victoria, Australia*
& *Cooperative Institute for Research in Environmental Sciences, University of Colorado Boulder, and NOAA/Earth System Research Laboratory, Boulder, Colorado*
** *University of Utah, Salt Lake City, Utah*

(Manuscript received 16 July 2012, in final form 8 May 2013)

ABSTRACT

This study presents a summary of the properties of deep convective updraft and downdraft cores over the central plains of the United States, accomplished using a novel and now-standard Atmospheric Radiation Measurement Program (ARM) scanning mode for a commercial wind-profiler system. A unique profiler-based hydrometeor fall-speed correction method modeled for the convective environment was adopted. Accuracy of the velocity retrievals from this effort is expected to be within 2 m s^{-1}, with minimal bias and base core resolution expected near 1 km. Updraft cores are found to behave with height in reasonable agreement with aircraft observations of previous continental convection, including those of the Thunderstorm Project. Intense updraft cores with magnitudes exceeding 15 m s^{-1} are routinely observed. Downdraft cores are less frequently observed, with weaker magnitudes than updrafts. Weak, positive correlations are found between updraft intensity (maximum) and updraft diameter length (coefficient r to 0.5 aloft). Negligible correlations are observed for downdraft core lengths and intensity.

1. Introduction

Substantial uncertainty in numerical weather simulations and global climate model (GCM) predictions of possible climate change can be attributed to the representation of the effects of deep cumulus convection. There are clear motivations toward accurate treatments of the moist convective life cycle that range from improved operational warn-on-forecast capabilities (e.g., Stensrud et al. 2009) to the critical role of capturing statistical convective storm characteristics in the context of GCM energy balance, cloud radiative properties, and the general circulation (e.g., Del Genio et al. 2005; Del Genio 2012). To ensure the fidelity of future climate predictions, the inability of current GCMs to properly resolve deep convection necessitates observations and detailed process studies to improve convective parameterization for the foreseeable future (e.g., Jakob 2010).

One important limitation when elucidating the complex interactions among storm dynamics, thermodynamics, and the microphysics of deep convection is the practical hazard associated with obtaining direct measurements from within intense convective environments (e.g., aircraft penetrating electrically active severe storms with possible hail cores). The emphasis of this study is on the observations of vertical velocities within deep convective storms that are of known interest as constraints to the connections among humidity, entrainment, and microphysical treatments of storm-resolving models (e.g., Ferrier, 1994; Milbrandt and Yau 2005; Del Genio et al. 2012). On GCM scales, these observations are considered to be of growing value for maintaining a continued progression from traditional mass flux–driven ensemble GCM parameterization modes (e.g., Arakawa and Schubert 1974) to ones that may better

Corresponding author address: Scott Giangrande, Atmospheric Sciences Division, Brookhaven National Laboratory, Bldg. 490D, Bell Ave., Upton, NY 11973.
E-mail: scott.giangrande@bnl.gov

DOI: 10.1175/JAMC-D-12-0185.1

differentiate the organized convection life cycle through additional complexity that includes parameterization of cumulus vertical velocities (e.g., Donner et al. 2001).

In situ aircraft penetrations have traditionally provided the best insights into convective storm dynamics, microphysical characterization, and thermodynamic characterization. A landmark contribution to the understanding of thunderstorm-core properties came from the Thunderstorm Project (TP; Byers and Braham 1949). In the years following TP, armored aircraft have sampled intense convective storms over a variety of continental-type, nonsevere-to-severe thunderstorms (hail producing), including cases in Florida (e.g., Smith et al. 1999), Montana (Musil et al. 1986), Oklahoma (e.g., Loney et al. 2002), Colorado (e.g., Sand 1976; Kyle et al. 1976; Miller et al. 1990; Brandes et al. 1995), and Argentina (Rosenfeld et al. 2006). Specific examples of detailed updraft profiling include the work of Marwitz (1973), who coupled weak-echo-region chaff release and surface radar to track updraft intensity above cloud base within storms over the U.S. high plains. Yet, direct aircraft measurements within intense-thunderstorm conditions are nonetheless rare and are limited by maximum aircraft altitude and endurance restrictions that undermine the ability to characterize adequately the vertical distribution, magnitudes, and dimensions of updrafts (of maximum vertical velocity values to several kilometers above the freezing level; e.g., Marwitz 1973). Flight paths through intense convective cores often require additional safety avoidance for ''hail'' hazards (e.g., 55-dBZ reflectivity-factor threshold limits) that prohibit flight into the strongest core elements.

Substantial characterization of updraft and downdraft kinematics has been reported for airborne studies within tropical noncontinental convection and hurricanes, as highlighted by the works of LeMone and Zipser (1980, hereinafter LZ), Jorgensen et al. (1985), Igau et al. (1999), Anderson et al. (2005), and others. Aircraft sampling of these cores is less problematic than continental counterparts because of weaker cores and an absence of significant-sized and large amounts of hail. In this way, these studies do not claim to represent deeper convective cores with updraft and downdraft intensities that routinely exceed $10\,\mathrm{m\,s^{-1}}$. For both continental and tropical regimes, aircraft instrumentation errors are minor (e.g., Lenschow 1976), with most uncertainty attributed to physical (noninstrument) process variability that includes off-center core penetrations, cloud evolution during the transit times between aircraft samples, and the overall representativeness of field campaign events.

Given known aircraft restrictions, there is a need to advance remote sensing solutions that encourage longer-term cumulative convective characterization to facilitate cumulus representation in models. This study explores one possible solution: extended deployments of radar wind profilers to estimate vertical air motions in convective systems. Utilization of the measurements from profiling radars within continental convective thunderstorms has provided unique insights into vertical velocity for decades (e.g., Battan and Theiss 1970; Lehmiller et al. 2001), including deeper convection in tropical/monsoonal and so-called break continental regimes (e.g., Cifelli and Rutledge 1994; Williams et al. 1995; May and Rajopadhyaya 1996, 1999; May et al. 2002; Uma and Rao 2009; Heymsfield et al. 2010). An obvious challenge is that profiling radars operating in Rayleigh-scattering regimes under precipitating conditions measure a Doppler velocity (air motion and hydrometeor fall speed) and not the ambient air motion directly. Thus, profiler retrieval uncertainty is contingent on accurately compensating for the bulk hydrometeor fall speed within the illuminated radar volume. Nevertheless, advancing these techniques may be of additional benefit toward validation of multi-Doppler radar methods (e.g., Ray et al. 1980). These multi-Doppler methods also capture multidimensional core velocity properties (and over much larger spatial domains) but must adopt several additional constraints because the vertical component of the velocity is not well sampled by traditional scanning-weather-radar tilts.

The U.S. Department of Energy Atmospheric Radiation Measurement Program (ARM) Climate Research Facility (Ackerman and Stokes 2003) in Oklahoma recently reconfigured its existing 915-MHz (UHF) wind profilers to operate in vertically pointing modes to take samples through deep convection passing overhead. New operating modes unique to these commercial Vaisala, Inc., 915-MHz UHF (33-cm wavelength) systems were implemented to match better the sampling requirements for capture of convective-core properties that are typical for warm-season Oklahoma convective storms. The dataset includes profiler observations collected during two extended ARM Oklahoma campaigns in 2009 and 2011. Although these profiler observations cannot replicate aircraft sampling, the study adopts several standard definitions for diameter, intensity of vertical motion, and mass flux from previous airborne efforts (e.g., LZ).

This paper is organized as follows. A detailed description of the ARM profiler systems, the new sampling modes, and the profiler-campaign datasets are provided in section 2. The profiler retrieval method that was developed to recover convective-core properties and possible uncertainty in that method are outlined in section 3. Results for this study are documented in section 4. The interpretation of Oklahoma results in comparison with

TABLE 1. UAZR operating parameters for the 2009 and 2011 ARM SGP field deployments.

915-MHz UAZR parameters	2009 (CASA)	2011 (additional mode; MC3E)
Pulse length (ns)	2833	400; 2833
PRF (Hz)	8333	10 000; 8333
Gate spacing (m)	200	120; 200
Max range (ARM imposed limit; km)	15	9.3; 15
Nyquist velocity ($m\,s^{-1}$)	20	14.7; 20
Temporal averaging (s)	5	3; 3

previous aircraft and profiler studies is found in section 5, and brief conclusions are listed in section 6.

2. Dataset

The ARM 915-MHz UHF wind-profiling radars are the primary instruments used for the vertical velocity retrievals in this study. These 33-cm-wavelength LAP-3000 Vaisala (Scintec AG) wind-profiler systems have a 9° beamwidth produced with a 2 m × 2 m square phased-array antenna and are designed for estimating lower-tropospheric horizontal winds from near the surface to below 6–8 km. Multiple wind profilers have been operating in Doppler-beam-swinging mode at the ARM Southern Great Plains (SGP) facility, with the first data recording starting in 1992. In recent years, the number of wind-profiler products requested from the ARM data archive has been decreasing, prompting discussions on whether traditional wind-profiler products were benefiting the research community. Thus, ARM wind profilers were reconfigured in their software to point only vertically and to collect data suitable for observing deep convective clouds. In this vertically pointing mode, we will refer to these wind profilers as UHF ARM zenith radars (UAZRs).

As part of a 2009 collaborative effort between ARM and the Oklahoma Collaborative Adaptive Sensing of the Atmosphere (CASA) campaign (e.g., McLaughlin et al. 2009), two UAZR systems were relocated to within the CASA domain (to Cement and Sterling in Oklahoma). The systems underwent a low-cost conversion to a vertical-pointing mode suitable for sampling the depth of typical Oklahoma convective storms (to 15 km) at high temporal and spatial resolutions. Modes were guided by previous tropical radar-profiling examples (e.g., Williams et al. 1995; Ecklund et al. 1999).

An assumption of UAZR "convective" modes is that Bragg echo returns are overwhelmed by Rayleigh returns in precipitating conditions. The modified UAZR modes have an uncoded pulse length of 2833 ns and a pulse repetition frequency (PRF) of 8333 Hz (425-m pulse length and 120-μs interpulse period). Because of limited bandwidth between the UAZR and the data archive, the total number of recorded vertical range gates was limited to 75, providing a maximum sampling range of 15 km at 200-m gate spacing. The UAZR Nyquist velocity was set at 20 $m\,s^{-1}$, sufficient to allow capture of stronger convective updrafts. The temporal resolution is 5 s, corresponding to 8 point × 128 point FFT spectral averages. A Monte Carlo simulation designed to replicate realistic spectra was performed to estimate the mean Doppler velocity uncertainty of this mode as described in Williams (2012). Results indicate that, in a nonchanging environment, mean Doppler velocity uncertainties are dependent on the observed signal-to-noise ratio (SNR) and spectrum width [as shown in May and Strauch (1989)]. For larger spectrum widths (>4–6 $m\,s^{-1}$) and SNR > 0–5 dB (both typical for convective cores), mean Doppler velocity measurement uncertainty is typically less than 0.2 $m\,s^{-1}$. At typical Oklahoma storm horizontal advection speeds (~15 $m\,s^{-1}$), this mode represents vertical Doppler velocity measurements with horizontal scales of less than 100 m. As with aircraft instrument uncertainties (e.g., Lenschow 1976), mean Doppler velocity uncertainties are probably dominated by physical changes in the vertical velocities over the 100-m resolution rather than by instrument measurement uncertainties.

Four UAZR systems were eventually relocated to the ARM SGP site for the Midlatitude Continental Convective Clouds Experiment (MC3E) in 2011. A short-pulse UAZR mode (400 ns; 10 000 Hz) with a maximum range of 9.3 km (120-m gate spacing) and a Nyquist velocity of 14.7 $m\,s^{-1}$ was added to the previous convective sequence, alternating with the original UAZR convective mode at approximately 3-s averaging windows. In preprocessing, profiler modes are merged into a single 6-s gridded product. The additional mode and shorter averaging did not significantly affect profiler sensitivity but did mitigate UAZR exposure to receiver saturation at the lowest levels (typically only below 1 km). The second PRF can also be exploited to perform moment-based dual-pulse-repetition-frequency techniques for velocity dealiasing (not required during this 2011 campaign). A summary of the UAZR campaign modes is provided in Table 1, and additional discussions on processing techniques are found in Tridon et al. (2013).

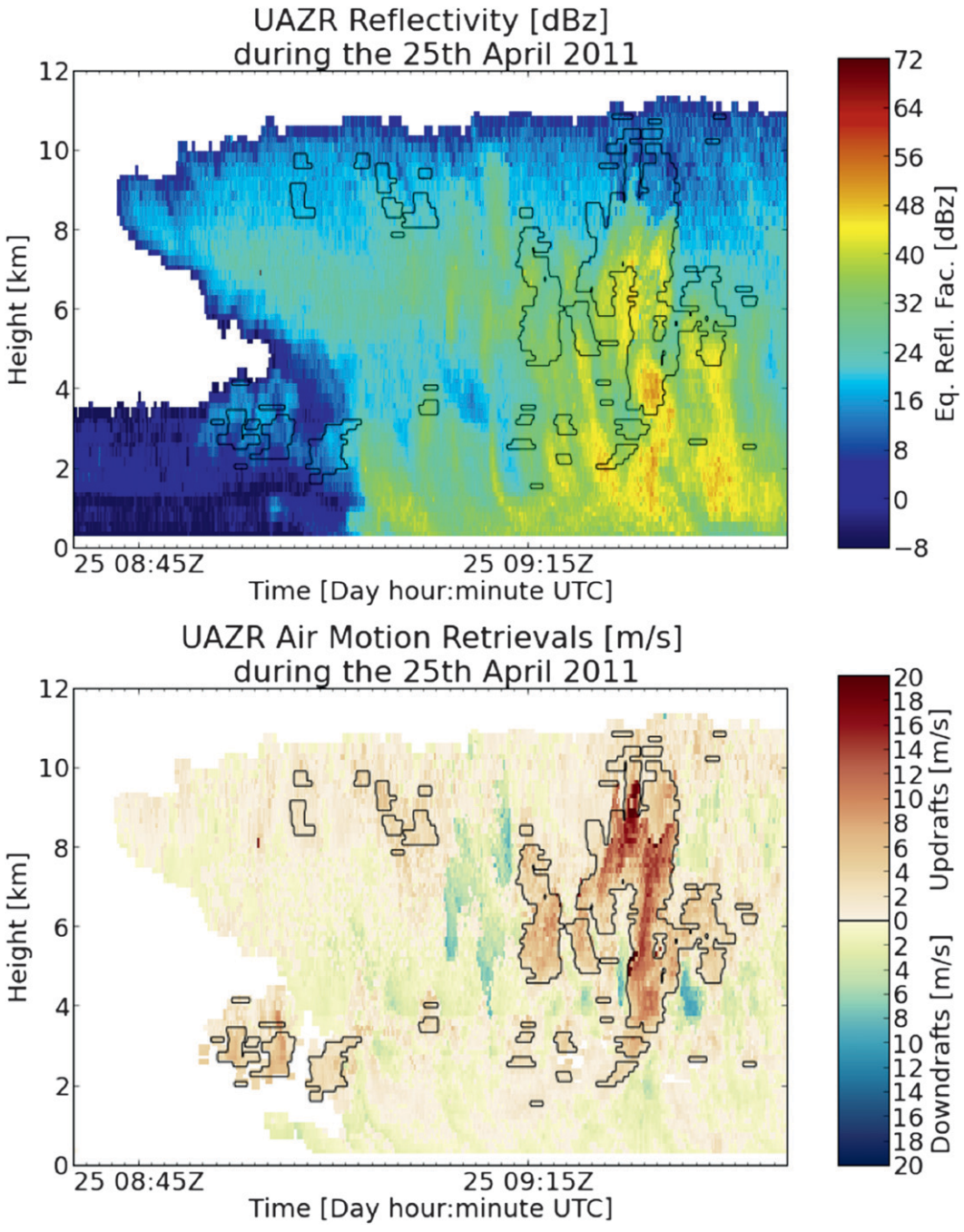

FIG. 1. Examples of (top) UAZR reflectivity factor and (bottom) mean Doppler velocity for the 25 Apr 2011 event during the MC3E campaign. Contours represent contiguous structures of updraft cores matching current 10-point threshold criteria.

Figure 1 provides an example of standard UAZR profiler reflectivity factor Z and mean Doppler velocity moments from the 25 April 2011 event. The full description of the UAZR dataset is found in Table 2. Additional ARM resources available during these two field campaigns included Joss–Waldvogel impact disdrometers (JWD; e.g., Joss and Waldvogel 1967) adjusted for known biases (e.g., Sheppard and Joe 1994) and collocated with UAZR systems. Calibration for UAZR Z was performed using relative comparison methods with sampled disdrometer Z values and nearby Next Generation Weather Radar (NEXRAD). Note

TABLE 2. List of ARM profiler events and NEXRAD-designated storm-motion vectors.

UAZR event	Event description	Convective cores (time, UTC)	Storm motion ($m\,s^{-1}$)
31 Mar 2009	Narrow convective line captured by single profiler	0000, 0100	8.5
29 Apr 2009	Embedded convective squall-line development over a single profiler	1000, 1100	17.5
5 May 2009	Isolated convective cell captured by a single profiler	1500	17.5
16 May 2009	Intense squall line captured by a single profiler	0200, 0300	13.5
4 Jul 2009	Isolated convective cells captured by single profiler	2300	5
30 Jul 2009	Isolated convective cells captured by a single profiler	0200, 0300	7.5
19 Aug 2009	Intense squall line captured by two profilers	0600	14
21 Oct 2009	Weak embedded squall line captured by a single profiler	1800	18
29 Oct 2009	Intense squall line captured by a single profiler	0900	29
25 Apr 2011	Isolated convective cells captured by a single profiler	0900, 1000	18.5
20 May 2011	Intense squall line captured by a single profiler	1000	17
23 May 2011	Isolated convective cells captured by three profilers	2100, 2200, 2300	17
24 May 2011	Isolated convective cells captured by two profilers	2100, 2200	23
12 Jun 2011	Squall line captured by four profilers	0500, 0600	15
16 Jun 2011	Squall line captured by four profilers	0800, 0900	16

that CASA and ARM SGP Central Facility domains were under the umbrella of several NEXRAD Weather Surveillance Radar-1988 Doppler (WSR-88D) instrumentsthat provided support for storm morphological behavior during this study. NEXRAD datasets were obtained through the quality-controlled National Severe Storms Laboratory National Mosaic and Multisensor Quantitative Precipitation Estimation (NMQ) gridded product archive (e.g., Zhang et al. 2005). Additional quality control for UAZR retrievals during MC3E was performed using collocated NOAA 449-MHz and 3-GHz profiling systems, which are discussed in the next section.

3. Methods for vertical velocity characterization in convective cores

Differences in spatial and temporal sampling imply profiler observations cannot replicate aircraft measurements. Therefore, seamless application of updraft/downdraft ''core'' definitions that are found in previous aircraft studies is a challenge. These kinds of definitions are required, however, for UAZR datasets to offer insights for improving model storm or multi-Doppler retrieval treatments of convection at similar resolution (to within $1\,km^2$). In this section, we detail an approach to characterize deep convective cores that is similar to that of LZ. For this study, we apply additional restrictions to LZ concepts to ensure appropriate UAZR capture of core properties. The following sections also describe our methods to map profiler mean Doppler velocity estimates to the ambient air motion. Core-size estimation and a discussion of the potential uncertainty associated with our methods are also presented.

Following the method of LZ, time series of profiler mean Doppler velocity observations along a specific height (range gate; approximately 75 height levels) are interpreted similarly to constant-altitude aircraft tracks through convection. In LZ, a core is defined as a region recording an air velocity $|v|$ that exceeds $1\,m\,s^{-1}$ for approximately 0.5 km. Given uncertainty considerations to follow, the UAZR demanded more stringent core requirements that are similar to those in previous profiler studies of May and Rajopadhyaya (1999). First, a more restrictive air velocity threshold ($|v| > 1.5\,m\,s^{-1}$) was established. The higher threshold is consistent with histogram analysis of UAZR profiler velocity data in predominantly stratiform versus convective conditions (not shown) and mitigates additional core designations that may only reflect a poor hydrometeor fall-speed correction (to be discussed in the following sections). The May and Rajopadhyaya (1999) profiler velocity studies utilized 1-min time-averaged profiler velocity values. The 1-min average is equivalent to approximately an average of 10 consecutive UAZR observations. For this study, we retain ''instantaneous'' UAZR Doppler velocity measurements (to better characterize extremes of individual cores) but necessitate that a valid core designation contain a minimum of 10 consecutive time observations exceeding the velocity threshold. For a modest convective-storm motion ($\sim 15\,m\,s^{-1}$ propagation) for the UAZR beamwidth, the 10 consecutive UAZR observations would be required to ensure capture of a 1-km-diameter core at an altitude of greater than 6 km. It is unlikely that smaller core sizes down to the 0.5-km

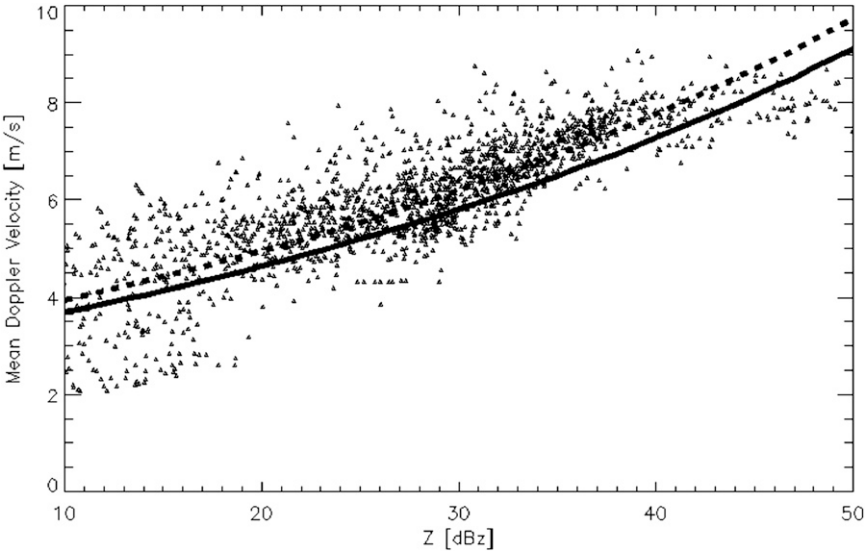

FIG. 2. Mean Doppler velocity vs reflectivity factor for JWD events during MC3E. The curves represent fall-speed relations that follow Steiner (1991) forms using coefficient $a = 2.95$ (solid curve) and $a = 3.15$ (dashed curve).

diameters reported by LZ can be captured faithfully using the UAZR system. Examples of contiguous updraft structures defined by following the current UAZR core definition are contoured on the UAZR fields in Fig. 1.

Mass flux calculations for this study follow basic LZ definitions and represent the rate of transport of mass per unit distance perpendicular to the profiler time/diameter dimension. These (air) mass flux values are determined by an expression (ρwD) that is the product of the air density ρ, the mean/median air motion w, and diameter D (herein, also referred to as length) of the core. This definition is a property of an individual core and is different from a ''traditional'' GCM-type definition for mass flux in cumulus parameterization that requires estimating the properties of all cores over a large area. Here, the statistics of a population of cores is a property of an ensemble of cores, with the properties of ensembles of cores still known to be of interest to larger-scale modelers (e.g., Donner et al. 1993).

a. Retrievals of air motion in rain

For vertically pointing UAZR systems, the mean Doppler velocity can be interpreted as the ambient air motion plus the weighted (positive downward) fall-speed contribution of the media within the radar volume. We estimate the fall-speed contribution using a standard Rayleigh-regime Z-based approach since an absence of a pronounced Bragg return at UAZR frequencies (as compared with Rayleigh returns) prohibits relying on Bragg features as a tracer for the ambient air motion. The coarse UAZR beamwidth coupled with convective turbulence (spectral broadening) also potentially limits additional forms of spectral air-motion estimates [e.g., left-edge methods, as discussed in Shupe et al. (2008), and other methods as in Cronce et al. (2007) and Campos et al. (2007)]. A similar synthetic approach to fall-speed estimation from aircraft-based radar observations was recently adapted to this challenge of convective-core velocity sampling in Heymsfield et al. (2010).

First, we adopt a power-law fall-speed relation studied by Steiner (1991) to estimate the reflectivity-weighted mean fall speed of rain:

$$V_f = aZ^b \quad (\mathrm{m\,s^{-1}}), \tag{1}$$

where $a = 2.95\,\mathrm{m\,s^{-1}}$, $b = 0.098$, and Z is the reflectivity factor in linear units ($\mathrm{mm^6\,m^{-3}}$). As reviewed by Steiner (1991), b-coefficient behavior in (1) is assumed to be stable. Figure 2 shows the scatterplot of mean reflectivity-weighted fall speed as a function of Z (dBZ) for the events of MC3E as sampled by the ARM JWD. If near-surface air motion is assumed to be negligible, the mean fall speed [calculated using standard drop fall-speed relations—e.g., fits to Gunn and Kinzer (1949)] gives one reference for bulk hydrometeor fall speed as a function of Z. In Fig. 2, the solid curve is following Steiner's (1991) a and b coefficients. The dashed curve represents a linear fit curve for $Z > 10\,\mathrm{dB}Z$ and suggests an a coefficient set to $3.15\,\mathrm{m\,s^{-1}}$ with the b coefficient unchanged from that in Steiner (1991). With this matched coefficient, the spread of observations is typically to

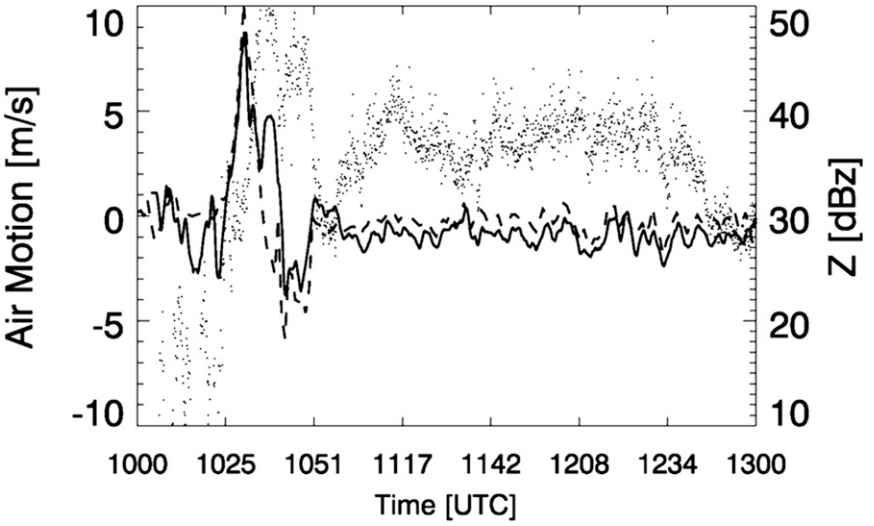

FIG. 3. Comparison of dual-frequency-profiler velocity retrievals (dashed line) vs UAZR retrievals (solid line) for the 20 May 2011 MC3E event. The data, including UAZR reflectivity factor values (dots), are from 1.5 km AGL.

within 0.5–1 m s^{-1}. This result, coupled with previous profiler studies and additional velocity checks within stratiform (weaker vertical motions) conditions, provides confidence in the capability of the retrieval to differentiate cores having $|v| > 1.5$ m s^{-1}. We note that this degree of uncertainty is similar to aircraft observations (absolute; e.g., LZ; Lenschow 1976). The offered disdrometer interpretation neglects possible uncertainty contingent on near-surface air motions, event-to-event drop size distribution (DSD) variability, and/or JWD sampling errors, however. It is assumed that these errors are of less importance when compared with the velocities expected in deep convective cores observed by vertically pointing radar.

As an additional quality check, the MC3E dataset provided several events that have collocated dual-frequency profiler observations (e.g., Williams 2012) at 3 GHz and 449 MHz. This frequency pair allows independent retrievals of air motions from the surface to the base of the melting level, capitalizing on the difference between Rayleigh and Bragg echo returns. Figure 3 displays one comparison sequence (1.5-km altitude; 20 May 2011) between dual-frequency velocity retrievals (dashed line), UAZR (residual) air-motion retrievals (solid line), and the reflectivity factor (dots). UAZR corrections are found to be within 1 m s^{-1} of the dual-frequency methods, showing solid agreement within an intense low-level updraft–downdraft couplet. Notable discrepancies between these retrievals, as shown in Fig. 3, are attributed to the likelihood of larger raindrops from larger melting aggregates in the trailing stratiform region (e.g., an event-specific DSD variability, wherein the Z-based methods tended to underestimate fall speeds by 0.5 m s^{-1}) and to errors in the dual-frequency technique's ability to resolve Bragg behaviors in heavily precipitating downdraft cores. The majority of dual-frequency retrievals at the lower levels indicate that near-surface air motions (retrievals within the lowest 1 km) seldom exceed $|v| > 1.0$ m s^{-1}, which is not unexpected for a dataset that is dominated by trailing stratiform rain conditions (not shown).

b. Retrievals of air motion in convection: Graupel

Applying Z-based fall-speed predictions above the freezing level in convective cores is nontrivial. Relationships as in (1) adapted to bulk dry ice and aggregated snow types are reliable for convective air motions since snowfall speeds are often less than 2 m s^{-1} (e.g., Protat and Williams 2011). "Snow" relationships are, however, complicated within deeper convective cores that include several species of frozen and mixed-phase hydrometeor of varying bulk density and, therefore, a wider range of possible fall speeds. Our study requires realistic behavior for convective graupel and/or small hail, common species that disproportionally influence the behaviors of bulk profiler Z versus fall speed when present near or above the freezing level.

Since limited graupel fall-speed insights are available and no direct observations of a pure graupel fall-speed–reflectivity-factor behavior exist, we elect to consider the results from a high-resolution convective storm model to establish an initial characteristic relationship for our Oklahoma convective environment. The model we use is a three-dimensional, fully compressible,

nonhydrostatic cloud model (the Straka Atmospheric Model; e.g., Straka and Mansell 2005). The particular simulation was one forced using an analytical thermodynamic sounding as in Weisman and Klemp (1982) that has a wind profile known to produce supercell storms. Our domain size is 105 km × 105 km × 20 km, with constant horizontal grid spacing of 150 m. To be certain, additional graupel behaviors and associated uncertainty might also be eventually explored by remote sensing platforms using particular pairings of profilers [50 and 2835 MHz, as in Protat and Williams (2011) for ice clouds]. To our knowledge, no reliable dataset at this profiler pairing exists within deeper continental storms. Thus, the offered modeling exercise is a baseline until improved insights are available. A relevant theoretical graupel approach has been previously attempted for aircraft-based observations at X-band (3 cm) wavelength (Heymsfield et al. 2010) that poses additional challenges (uncertainty) in deep convective cores as a consequence of significant non-Rayleigh scattering and attenuation in rain near Earth's surface. These factors are not as significant at UAZR wavelengths.

Our model adopts a microphysical parameterization scheme that builds upon the bulk parameterization designed by Straka and Mansell (2005) toward a three-moment scheme (e.g., Milbrandt and Yau 2005) that includes treatment for 10 ice-crystal habits. The first five habits are considered to be ''small'' ice particles and feature frozen cloud droplets, bullet rosettes, columns, dendrites, and plates. The second five habits are ''large'' ice habits and include dry snow aggregates, graupel, frozen raindrops, and two hail categories (originating from either graupel or frozen drops). Graupel in this model is initiated with a density of 300 kg m^{-3} and originates from highly rimed frozen drizzle, ice crystals, or snow aggregates. The two hail species are initiated with density of $\geq$700 kg m^{-3} and sizes that range from 9 to 51 mm in diameter.

The point of interest for our current UAZR profiler study when adopting this particular parameterization scheme is in the prediction of ice particle densities r_x at temperatures below freezing. Here, prediction of ice density is performed for each of the large ice habits. The basic formulation for this prediction is as follows. First, the advection and diffusion of total number concentration N_T, mixing ratio Q, reflectivity factor Z, and, if appropriate, larger ice particle densities are computed with the International System of Units (SI) for each hydrometeor species x with

$$\frac{\partial N_{T,x}}{\partial t} = -u_i\frac{\partial N_{T,x}}{\partial x_i} + \frac{\partial}{\partial x_i}\left[\rho K_h\frac{\partial (N_{T,x}/\rho)}{\partial x_i}\right] + \frac{\partial(\overline{V_{TN,x}}N_{T,x})}{\partial x_3} + SN_{T,x}, \tag{2}$$

$$\frac{\partial Q_x}{\partial t} = -\frac{1}{\rho}\frac{\partial \rho u_i Q_x}{\partial x} + \frac{Q_x}{\rho}\frac{\partial \rho u_i}{\partial x_i} + \frac{1}{\rho}\frac{\partial}{\partial x_i}\left(\rho K_h\frac{\partial Q_x}{\partial x_i}\right) + \frac{1}{\rho}\frac{\partial(\rho\overline{V_{TQ,x}}Q_x)}{\partial x_3} + SQ_x, \tag{3}$$

$$\frac{\partial Z_x}{\partial t} = -u_i\frac{\partial Z_x}{\partial x_i} + \frac{\partial}{\partial x_i}\left(K_h\frac{\partial Z_x}{\partial x_i}\right) + \frac{\partial(\overline{V_{T,x}}Z_{T,x})}{\partial x_3} + SZ_x, \tag{4}$$

and

$$\frac{\partial \rho_x}{\partial t} = -u_i\frac{\partial \rho_x}{\partial x_i} + \frac{\partial}{\partial x_i}\left(K_h\frac{\partial \rho_x}{\partial x_i}\right) + \frac{\partial(\overline{V_{T,Q}}\rho_x)}{\partial x_3} + S\rho_x, \tag{5}$$

where t is time; x_i or x_j are the Cartesian directions x, y, and z; u_i are the Cartesian velocities u, v, and w; and ρ is the dry density of air. Note that $V_{T,x}$ is the mass-weighted terminal fall speed of the distribution of hydrometeor species x. The mixing coefficient used for scalar variables is given by $K_h = 3K_m$, where K_m is the mixing coefficient for momentum (different values for this coefficient are also possible and would follow from 1/Pr, where Pr is the Prandtl number). The S terms in expressions (2)–(5) are the source and sink terms. Finally, a new density of ρ_x is predicted by the following:

$$\rho_x^{n+1} = \frac{\rho_x^n Q_x^n + \Delta t\left(\rho_{x,\mathrm{conv}}^n\left.\frac{dQ_x}{dt}\right|_{\mathrm{conv}}^n + \rho_{x,\mathrm{rime}}^n\left.\frac{dQ_x}{dt}\right|_{\mathrm{rime}}^n + \rho_I^n\left.\frac{dQ_x}{dt}\right|_{\mathrm{rain}}^n + \rho_{m,\mathrm{ice}}^n\left.\frac{dQ_x}{dt}\right|_{m,\mathrm{ice}}^n + \rho_x^n\left.\frac{dQ_H}{dt}\right|_{\mathrm{sub/dep}}^n\right)}{Q_x^n + \Delta t\left(\left.\frac{dQ_x}{dt}\right|_{\mathrm{conv}}^n + \left.\frac{dQ_x}{dt}\right|_{\mathrm{rime}}^n + \left.\frac{dQ_x}{dt}\right|_{\mathrm{rain}}^n + \left.\frac{dQ_x}{dt}\right|_{m,\mathrm{ice}}^n + \left.\frac{dQ_H}{dt}\right|_{\mathrm{sub/dep}}^n\right)}, \tag{6}$$

where n is a time level, Q is mixing ratio (kg kg^{-1}), ρ_{conv} is the density with conversions, and $\rho_{\mathrm{sub/dep}}$ is the sublimation/deposition density (assumed to be the density of the ice particle). The rime density ρ_{rime} from (6) is a function of the impact velocity, temperature, and cloud droplet size. It is given by

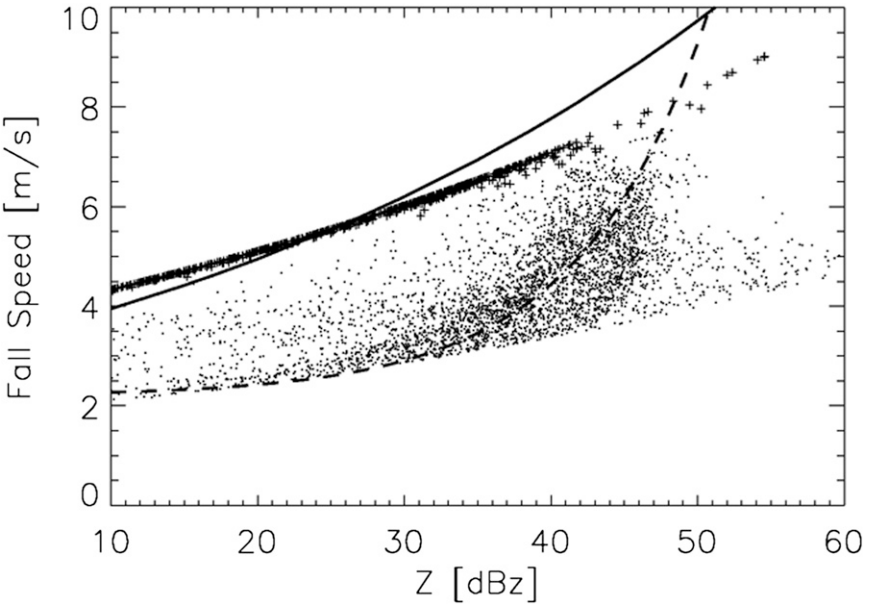

FIG. 4. Scatterplot of modeled behavior of graupel fall speed vs reflectivity factor. Plus signs represent modeled graupel having higher density (>800 kg m^{-3}). The solid curve is the rain relation from (1). The dashed curve is our assumed graupel fit from (8).

$$\rho_{\text{rime}} = 300\left(\frac{-R_{\text{CW}}V_{T,\text{impact}}}{T_{\text{sfc}}}\right)^{0.44}, \qquad (7)$$

where R_{CW} is the radius of cloud droplets, $V_{T,\text{impact}}$ is the impact velocity, and T_{sfc} (°C) is the surface temperature of ice particles that are riming. The temperature is the ambient air temperature during dry growth, which may underestimate the ice particle's surface temperature. Note also that rime density is not computed during wet growth. The maximum rime density is 900 kg m^{-3}, and the minimum rime density is 170 kg m^{-3}.

Figure 4 displays the predicted scatterplot of UAZR behavior for the mean reflectivity-weighted fall speed versus the reflectivity factor of graupel obtained from this model. Fall speeds are adjusted to sea level pressure. The lowest-density graupel behaviors (<200 kg m^{-3}) are removed because they are believed to be a less realistic depiction of the deeper convective cores. The solid curve in Fig. 4 is the ''rain'' relationship from (1) with $a = 3.15$ m s^{-1}. The dashed curve follows

$$V_f = 2.2 + \{10^{[Z\,(\text{dBZ})-33.0]/10.0}\}^{1/2} \quad (\text{m s}^{-1}), \qquad (8)$$

where Z is the associated graupel reflectivity factor (dB).

High-density graupel (density > 800 kg m^{-3}) and small hail are also important fall-speed behaviors to capture for convective cells. The simulation modeled higher-density graupel but only to within close proximity of the freezing level (within 500 m; plus signs in Fig. 4). The simulated higher-density graupel and small hail in the vicinity of the freezing level behaved fortuitously similarly to the rain fall-speed prediction from (1) and often to within 2 m s^{-1}. The discrepancies are possibly less important when considering mixtures of these media in convective cores near the freezing level (or avoidance of heights having possible melting-layer contamination). Figure 4 implies a crossover from lower- to high-density graupel behavior at $45 < Z < 50$ dBZ. As with the empirical rain relationship, (8) is relatively insensitive to modest radar miscalibration, suggesting errors to within 0.5 m s^{-1}. The spread of graupel behaviors in Fig. 4 highlights a model reflectivity–based relationship having uncertainty to within 2 m s^{-1}. This result is not surprising, considering intrinsic modeled graupel fall-speed behaviors (in the absence of hail) do not vary too significantly from the lower to higher densities (cf. Straka and Mansell 2005, their Fig. 1). Overall, we do not anticipate significant (>2 m s^{-1}) uncertainty in averaged velocity profile behaviors if following relation (8) in graupel regions provided that the radar Z measurements are unbiased and averaging is performed over an extended dataset. The behavior of (8) is similar to the previous Heymsfield et al. (2010) relationship form for graupel (allowance for wavelength-specific mean Doppler velocity and Z calculations), for which those

authors suggest an uncertainty that is often less than $2\,m\,s^{-1}$. Again, X-band aircraft radar systems face more significant challenges (radar based) in appropriately modeling Z for non-Rayleigh scattering, graupel, rain–hail mixtures, and attenuation in rain.

c. Synthesis of fall-speed corrections and core classification

This study adopts a synthetic approach to estimate vertical air motions and isolate the statistics of deeper convective cores. Since fall-speed corrections require some knowledge of the bulk hydrometeor type (e.g., rain, graupel, hail, or dry snow), corrections are applied contingent on the results of a hydrometeor classification scheme developed for the UAZR system. The classification of UAZR profiler observations helps to mitigate nonmeteorological contaminants (e.g., Bragg scattering) and avoid extended stratiform regions for which fall-speed relationship-retrieval uncertainty [e.g., (1)] would be of similar magnitude to the air motions (e.g., Yuter and Houze 1995).

The classification is performed following traditional radar-based classification concepts (e.g., fuzzy logic; Straka et al. 2000), methods of profiling with aircraft radar (Geerts and Dawei 2004), and other radar-based convective/stratiform moment ranges (e.g., Z-based thresholds; Steiner et al. 1995). A similar profiler-based convective/stratiform classification scheme at the S-band (10 cm) wavelength has been already developed by Lerach et al. (2010). The primary complication at the UAZR wavelength as compared with S band is a requirement for the identification and removal of Bragg echo contaminants. Otherwise, standard S-band convective/stratiform considerations having additional radiosonde support have been shown to segregate efficiently the bulk boundaries among ''convective rain,'' ''stratiform rain,'' ''dry snow'' (dry aggregates or lower-density crystals), and/or ''convective graupel'' regions for the requirements of this effort. Similar to the Lerach et al. (2010) method, UAZR spectrum-width values (larger beamwidth) exceeding $3\,m\,s^{-1}$ are assumed to be consistent with convective turbulence. The relatively modest number of UAZR events allowed an additional manual check of each profiler classification to ensure the isolation of deep convective-core regions from so-called brightband-topped stratiform rain regions or possible Bragg contaminants.

To the specific challenge of Bragg echo identification, fuzzy-logic membership functions assigned the highest confidence to lower $Z < 30\,dBZ$, low Doppler velocity $|v| < 1.5\,m\,s^{-1}$, and low UAZR spectrum width $< 1.5\,m\,s^{-1}$ echoes. Bragg echoes are typically assumed to be weak in comparison with deeper precipitation echoes, tracing air motions corresponding to clear-air conditions. On the basis of these criteria, Bragg echoes most directly conflicted with weaker dry-snow echoes that similarly favored such radar moment behaviors (e.g., Lerach et al. 2010). For the UAZR events, a practical solution was to assume that prominent Bragg echo identifications are allowable only at lower altitudes below 4 km (or sounding-based freezing level).

Expressions (1) and (8) are subsequently applied as the correction for hydrometeor fall-speed contingent on the results of bulk classification. Below the melting level, rain fall-speed corrections adopt the relationship from (1). Starting at 500 m above the freezing level, the fall-speed correction for convective graupel is according to (8) for $Z < 50\,dBZ$ and then follows (1) for $Z > 50\,dBZ$. Dry snow, occasionally classified at the peripheries of the convective cores, is assumed to fall at $1\,m\,s^{-1}$. All velocities are subject to adjustments for air density at altitude according to the formulation of Foote and duToit (1969).

d. Core-diameter estimation: NEXRAD

LZ describe core-diameter length in the aircraft context as the product of the duration of the identified core and the aircraft speed. In this study, we define the core diameter as the product of convective-storm motion and the duration of the designated core observation. Once again, values of air mass flux are determined by the expression ρwD that is the product of the air density, the air motion, and the diameter of the core, respectively. For the storms in Table 2, storm advection speed is estimated assuming that the NEXRAD Mosaic reflectivity field moves without deformation [the so-called stationarity hypothesis in Gal-Chen (1982)]. In practice, and especially for the current study focusing on convective cells, this assumption is never perfectly satisfied, given the short lifetime of convective cells. Our objective is therefore to retrieve the translational velocity vector $\mathbf{V0}(u0, v0)$ that minimizes in the least squares sense the difference between reflectivity fields from two or three consecutive volumetric radar scans of interest (one average estimate provided for each event). The inversion problem is solved using the variational formalism, as described in Laroche and Zawadzki (1994) and Protat and Zawadzki (1999).

Reflectivity fields are only from those cores having a relatively higher $Z > 20\,dBZ$ at a lower height (2 km) to avoid anvil propagation in opposing directions at higher elevations. The use of different thresholds between 20 and 30 dBZ resulted in only small differences in the advection speeds ($<1\,m\,s^{-1}$). The resulting storm-motion estimates are listed in Table 1 and range from 5 to $29\,m\,s^{-1}$. Given vertical wind sheer, the estimates

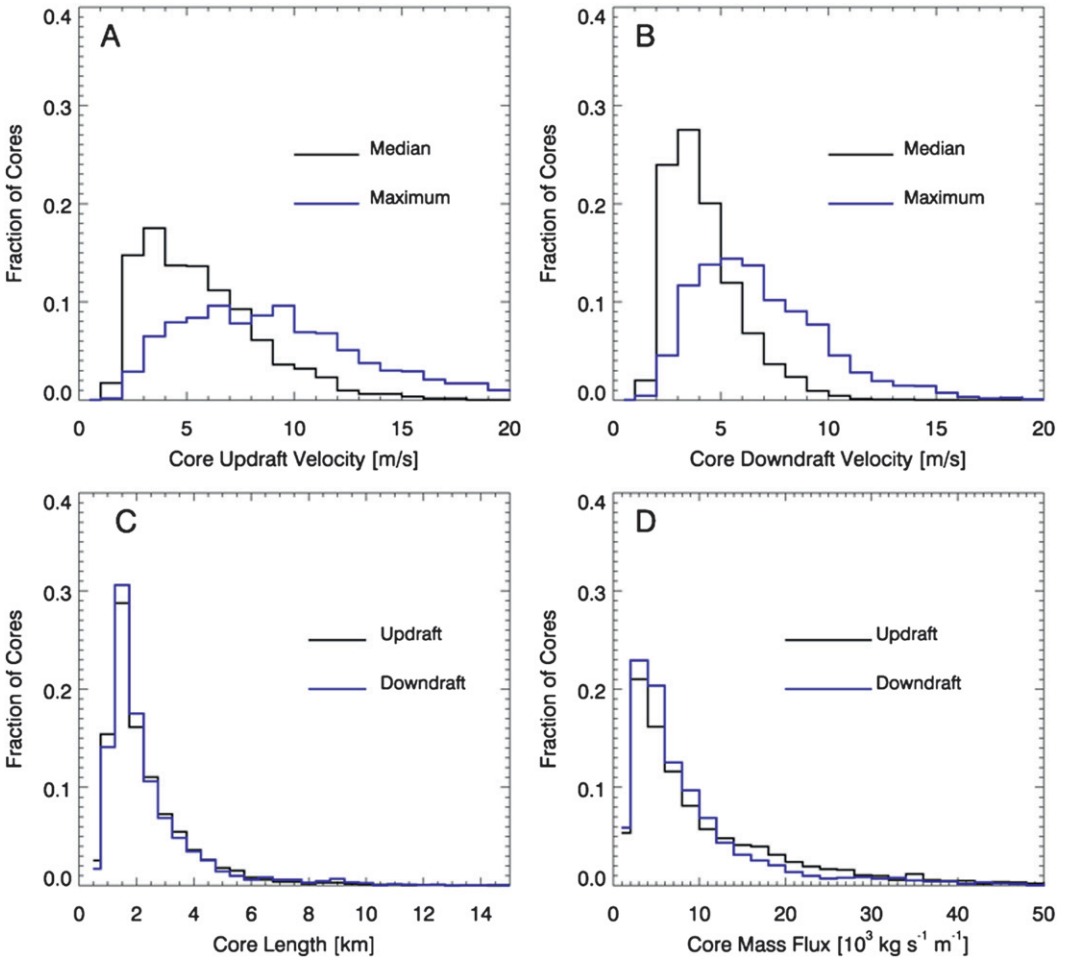

FIG. 5. One-dimensional frequency histograms for updraft and downdraft core properties of (a) median and (b) maximum core velocities, (c) core diameter, and (d) core mass flux.

reflect a limited storm behavior and there is no inherent storm-motion ''truth.'' Thus, some uncertainty in core-diameter sizing as well as mass flux is expected contingent on the associated errors when tracking precipitation cores. If errors in storm-core motions can be considered as unbiased, the overall exposure of core-diameter and mass flux estimates to such tracking uncertainty can be mitigated through extended dataset averaging. More persistent $3\,m\,s^{-1}$ errors (e.g., representing a 20% error of the average dataset storm motion of $15\,m\,s^{-1}$) imply an uncertainty in core-diameter estimates of around 20% (here, also contingent on event-specific storm motion, evolution, and possible profile biases).

4. Results

For events listed in Table 1, standard LZ-type properties of core diameter, median, and maximum velocity and mass flux are computed. In total, approximately 4000 updraft cores and 3000 downdraft cores were designated between the heights of 1 and 12 km using a requirement of 10 consecutive profiler points (approximately 60 s in time) that meet the criterion of $|v| > 1.5\,m\,s^{-1}$. The number of designated cores following this approach is understandably larger than the counts typically attributed to aircraft studies [e.g., as reviewed by Anderson et al. (2005)] as a consequence of high-resolution UAZR height-sampling capabilities (200-m gate spacing). The number of unique, contiguous time–height structures (as contoured in Fig. 1) containing these ''horizontal'' aircraft-style core definitions is substantially lower.

Figures 5a–d illustrate one-dimensional frequency histograms for updraft-core and downdraft-core properties. It is clear that the distributions of median and maximum velocities for updrafts are less positively skewed than those for downdrafts, indicating that

updrafts more frequently achieve higher magnitudes. The relative frequencies of the updraft and downdraft core lengths are, however, similar. It follows that since there is a much larger spread of the velocity values associated with updraft cores there should also be a wider range distribution for the updraft mass flux (Fig. 5d). Additional sensitivity testing revealed that adopting a less stringent time criterion of five consecutive data points doubled our number of core designations (including possible fraudulent core designations). The influx of small, sub-1-km cores exhibited median and maximum $|v|$ of $<10\,\mathrm{m\,s^{-1}}$, with properties being similar for both updrafts and downdrafts. These findings within likely less-significant, turbulent features suggest that our retrieval methods did not appear to preferentially favor core updrafts or downdrafts.

a. Combined velocity-profile statistics

Velocity-core statistics are summarized according to 500-m altitude bins starting at an altitude of 1 km above the surface. For each height level, the cumulative series of core diameters, median velocity, and mass flux are ranked by magnitude. Figures 6a–c plot updraft cores according to their median (lines with diamonds), 90th-percentile level (lines with triangles), and 95th-percentile level (lines with asterisks). For this study, it was found that the number of updraft cores is roughly equally distributed between the altitudes of 2 and 10 km, having fewer observations near the surface and to the tops of storms (not shown). Figures 7a–c provide similar profiles for the downdraft-core statistics. Downdrafts are more frequently observed at the lower altitudes to approximately 1 km above a typical freezing-level height (5 km), at approximately double the number observed for these heights as compared with above the freezing level.

b. Comparisons of velocity versus core diameter

Of key interest for convective parameterizations is the connection between the updraft size and the intensity of the core. Figures 8a–d show scatterplots and accompanying 2D histogram count contours for joint velocity and core-diameter length pairings. The associated Pearson linear correlation coefficients r have also been calculated for these datasets, recording correlations that are weak or possibly at insignificant levels. The correlations are always positive, with the highest correlation observed for the updraft core diameter and its relationship to its maximum core intensity ($r = 0.43$). The lowest correlations are found for the median downdraft core velocity and its associated core length ($r = 0.19$).

Marginal improvements to these correlations result when the methods are stratified according to altitude.

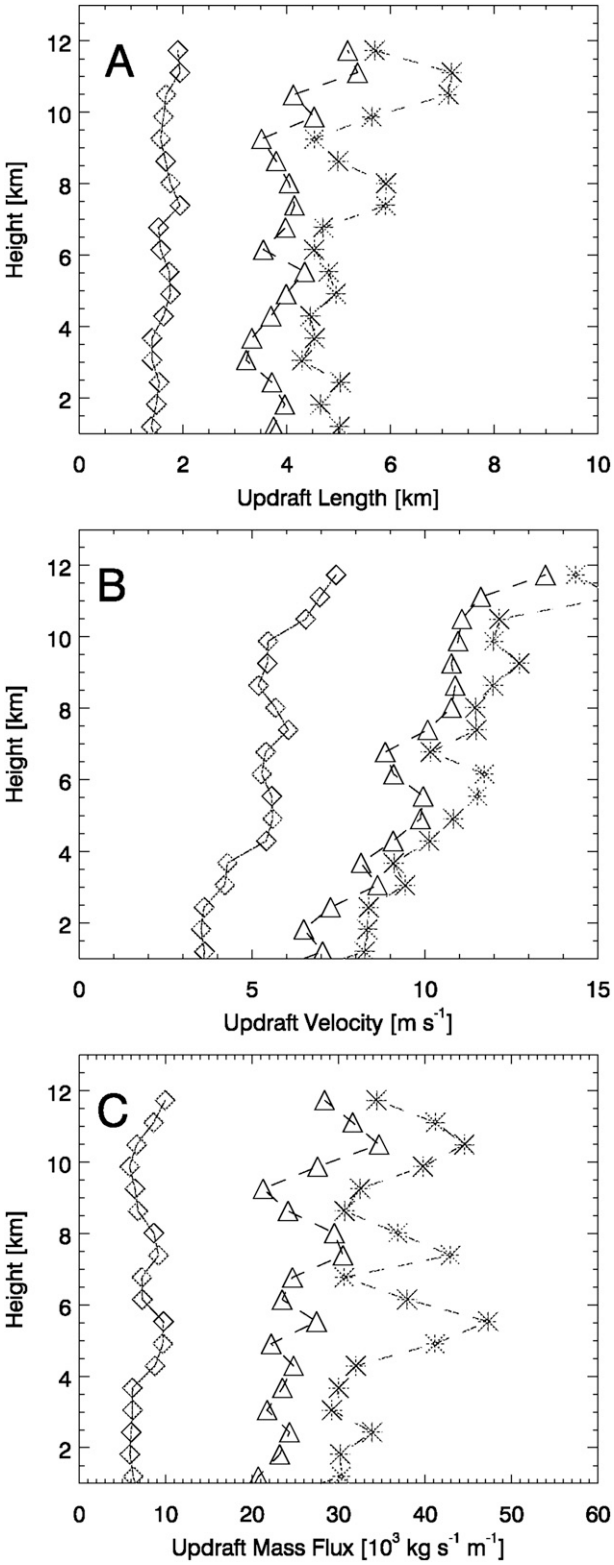

FIG. 6. Profile statistics of (a) updraft diameter, (b) median velocity, and (c) mass flux according to the median or 50th percentile (lines with diamonds), 90th percentile (lines with triangles), and 95th percentile (lines with asterisks).

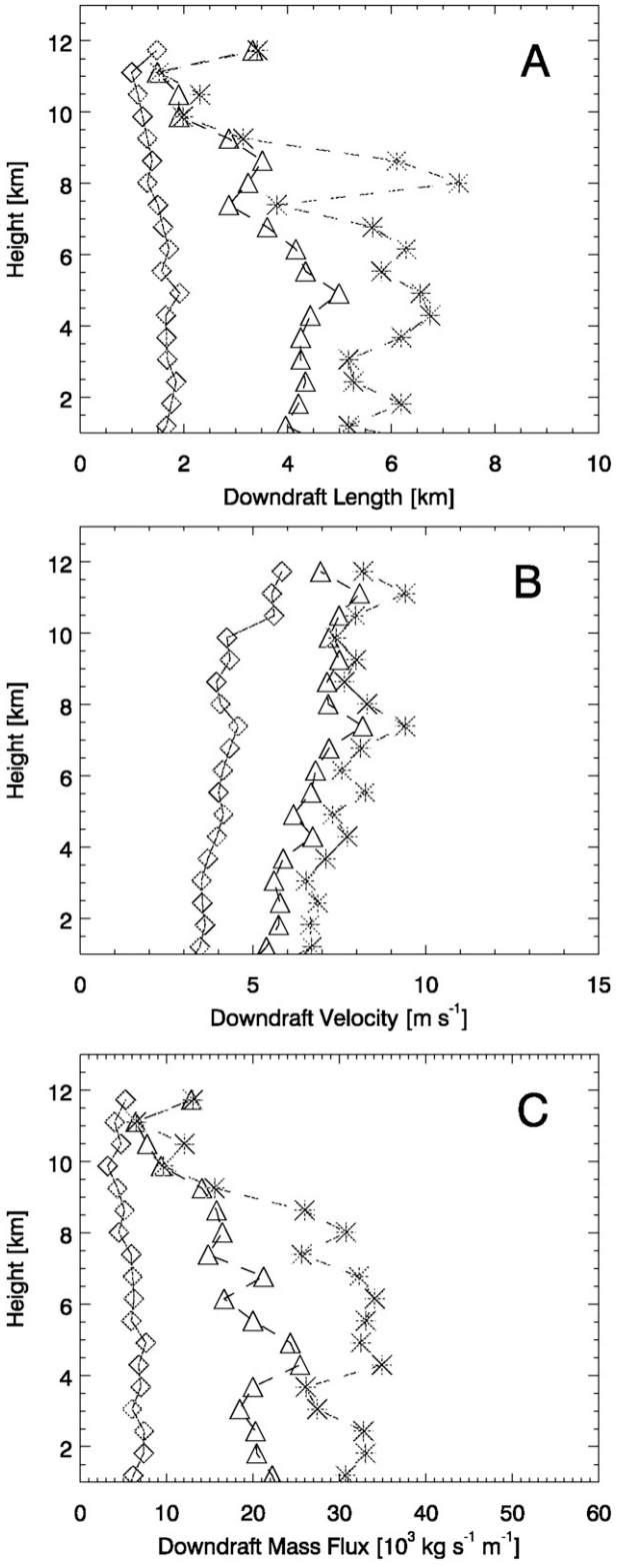

FIG. 7. As in Fig. 6, but for downdraft profiles.

Downdrafts located below the melting layer exhibit an apparent higher correlation (approximately $r = 0.3$). Updraft correlations conditional to maximum cores found above the freezing level are the most significant ($r = \sim 0.5$). The interpretation for these weaker correlations is complex, but the authors note that extremely high correlations are not necessarily expected. We specifically caution that one-dimensional sampling of ''triangular'' cores (e.g., those suggested in LZ) can be demonstrated to bias the observations of intensity, diameter, and mass transport (e.g., Jorgensen et al. 1985). As a consequence, these 1D sampling biases could act to lower the apparent correlations between updraft parameters.

c. *Mass flux observations with diameter*

Figure 9 plots the two-dimensional probability density function of mass flux behaviors, partitioned according to percentage of the observed mass flux attributed to a particular core diameter and height interval. Note that approximately one-half of the core mass flux observed from the UAZR observation dataset was associated with cores with an estimated diameter of 2 km or smaller and that nearly 80% of the observed mass flux is associated with estimated diameters that are smaller than 4 km. As a function of height, updraft behaviors (Fig. 9, top) indicate that the mass flux is well distributed in our observations, peaking at the midlevels. As anticipated by the limited number of downdraft core designations at the higher altitudes, a majority of the downdraft mass flux observations were located at the lower levels and typically below the melting level (5 km). Downdraft mass flux is distributed across a wider range of diameter sizes relative to the updraft mass flux.

Figure 10 shows the updraft and downdraft mass fluxes plotted as a function of the core length for the median, with the 90th- and 95th-percentile velocity values plotted according to similar conventions. As expected, fewer large cores are observed for this dataset, but the larger cores are those associated with the largest values of mass flux (according to the mass flux definition adopted by the current study). Updraft mass flux is found to be larger than downdraft mass flux for similar-sized cores, consistent with additional intense-core-velocity observations as previously shown for distributions in Fig. 5.

5. Comparison of UAZR profiler results with other studies

The most relevant dataset to compare with this UAZR study is the findings of the Thunderstorm Project (e.g., Byers and Braham 1949, chapter 2). As with TP

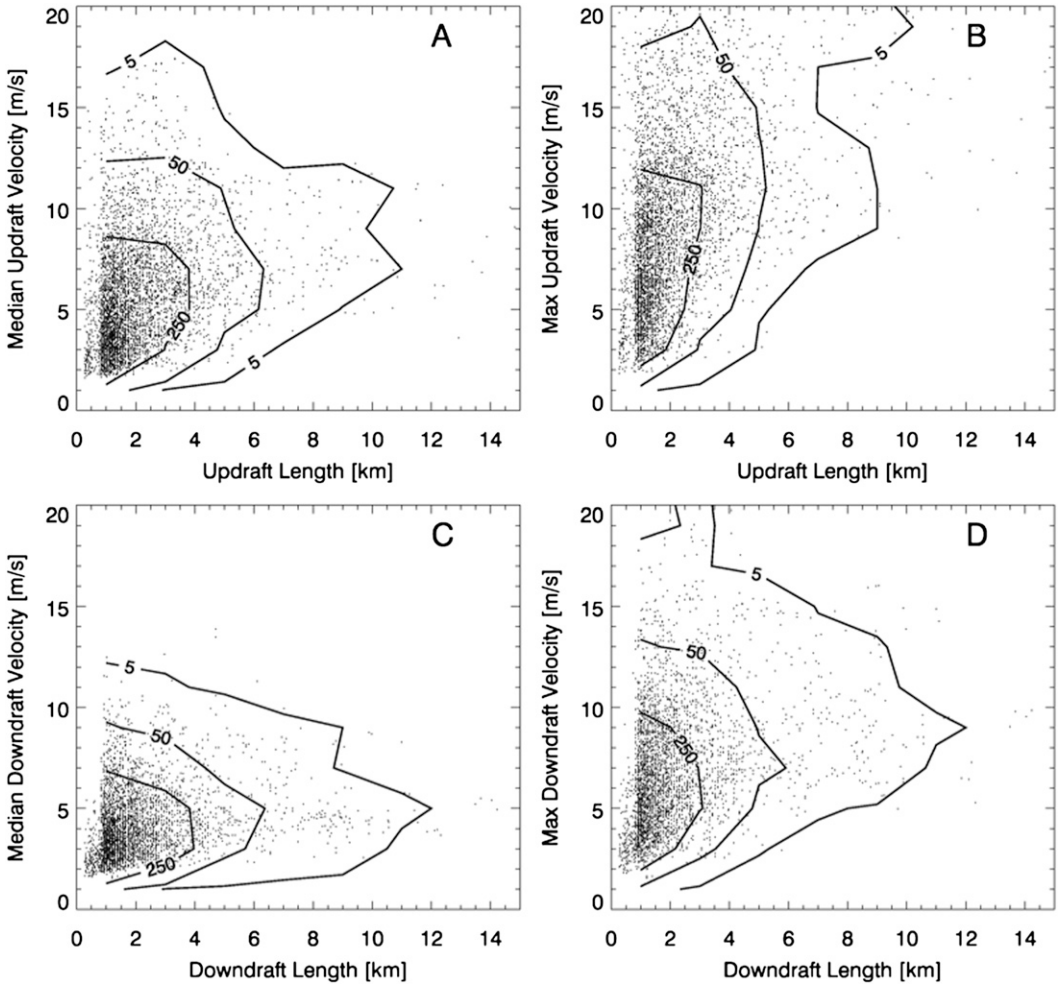

FIG. 8. The 2D histograms (individual points with observational frequency contours) of (left) median and (right) maximum velocity vs core diameter for UAZR for (a),(b) updrafts and (c),(d) downdrafts.

aircraft datasets, the strength of the UAZR observations is the ability to sample convective cores to high altitudes above the freezing level. These higher-altitude observations are rare for continental convective studies, as are the observations of stronger updrafts and downdrafts aloft. UAZR updraft profile behaviors for the median and higher-percentile core velocity values (as in Fig. 6) are consistent with the magnitudes and profile shape from TP. Also similar to TP, updraft intensity increases through the freezing level to the upper troposphere. Tropical core observations such as those of LZ show core updraft intensity increasing at least up to 3–4 km. It is noted that recent large-eddy simulation (LES) results (Khairoutdinov et al. 2009), which otherwise agree well with LZ's observations, appear to show updraft core intensity increasing to about 6 km. Convective-core velocity observations over land have also been reported by Heymsfield et al. (2010) to heights above 10 km. For these continental convective cases (southeastern United States), the ''mean'' profile of maximum (updraft) vertical velocity appears to steadily increase to a height above 10 km (velocity maximum peaking on average near 12 km; possible dry midlevel environments), again consistent with our UAZR 90% and 95% observations. The land-based updraft values that were reported by Heymsfield et al. (2010) often exceed 15 m s^{-1} (up to 30 m s^{-1}), which is also in agreement with UAZR observations.

The relative frequency at which updrafts are observed is approximately consistent with height. This UAZR result agrees well with the tropical profiler findings of May and Rajopadhyaya (1999). As opposed to tropical campaigns, however, it is common that continental datasets feature maximum core velocities that exceed 15 m s^{-1}. Cross comparisons of the UAZR with nearby profiler observations (Fig. 3) also indicate a likelihood of

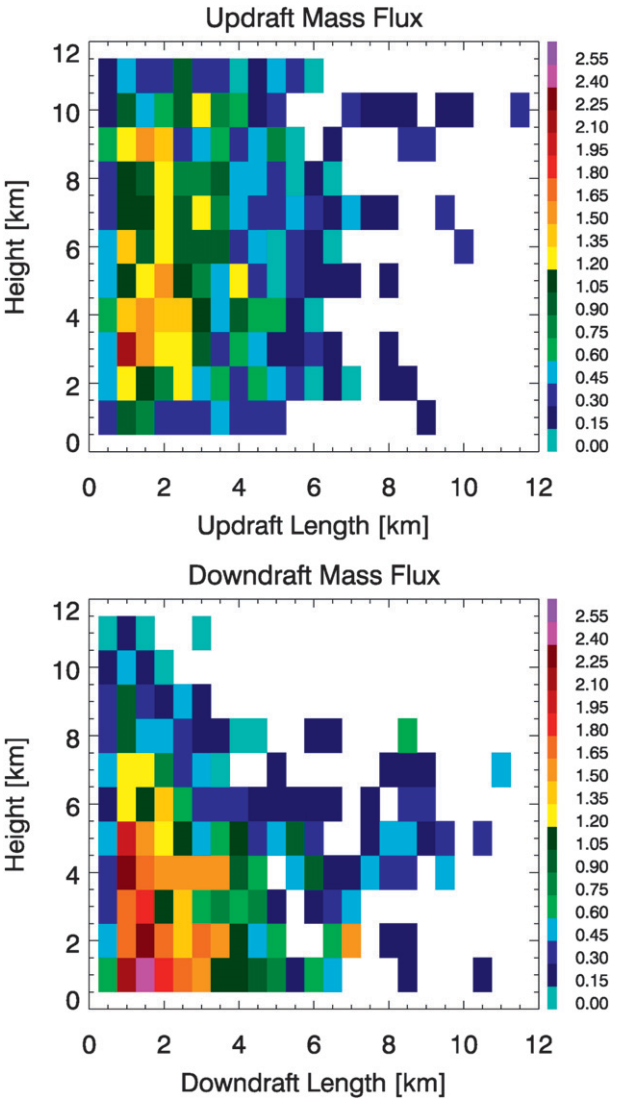

FIG. 9. The 2D probability density function of mass flux behaviors (percent of mass flux observed) from UAZR (top) updraft and (bottom) downdraft core observations.

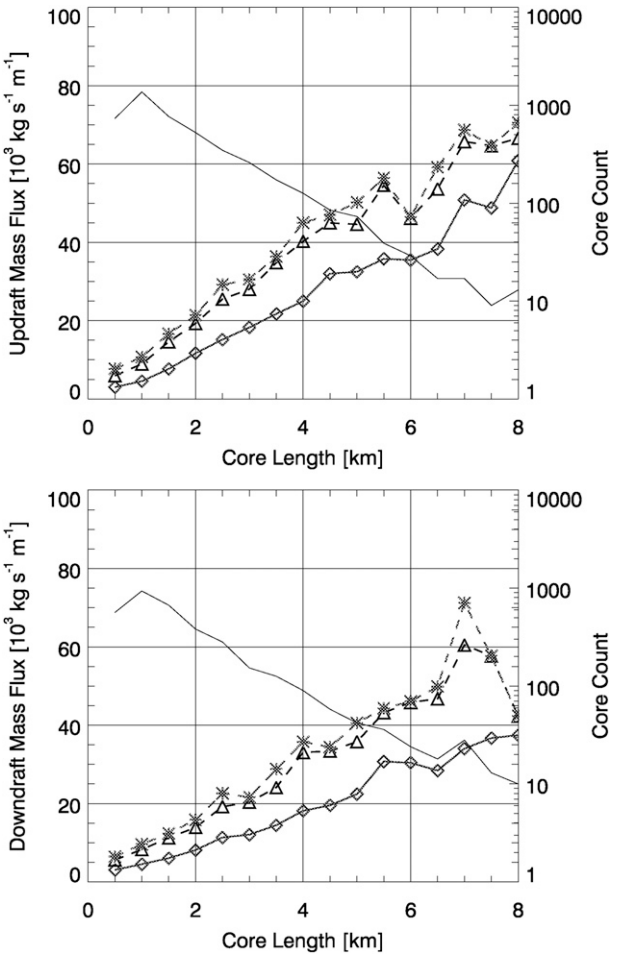

FIG. 10. (top) Updraft and (bottom) downdraft mass fluxes as functions of core length according to the median (lines with diamonds) and the 90th (lines with triangles) and 95th (lines with asterisks) percentiles. Core counts (thin solid lines) are included on the right ordinate axis.

strong maximum updraft cores of greater than 10 m s^{-1} even at low altitudes of less than 2 km (often below previous aircraft study coverage). That the UAZR and other independent profiling references witness such events provides a solid indication of the existence of stronger low-level cores, confidence in their intensity, and a possible role for upward mass transport at lower levels. The dataset updraft mass flux (observed histograms and probability density function) favored modest core sizes (1–3 km in diameter) at the mid- to upper levels (between 3 and 9 km AGL). The current UAZR dataset may still be limited and may require additional sampling because it may not represent the strongest convective cores given that maximum velocity estimates rarely exceeded 25 m s^{-1}. This situation is also evident in that substantial UAZR velocity dealiasing routines were not required for this dataset.

In previous studies, including LZ, downdraft-core properties are limited and/or often reported with behaviors that do not follow the findings of TP. To the authors' knowledge, the current UAZR study is unique with respect to continental downdraft-core behaviors since TP. Methods, including those of Heymsfield et al. (2010), for profiling may be increasingly limited toward Earth's surface as a consequence of attenuation in rain, whereas UAZR observations may alleviate possible discrepancies with those previous TP findings. UAZR downdraft cores can be summarized as follows: 1) Downdraft distributions indicate that downdraft cores are smaller and weaker than updrafts. 2) The frequency of downdraft-core observations sharply decreases above

the freezing level. 3) Downdraft cores are still observed to heights above 8–10 km, with 4) the magnitudes of downdrafts still achieving significant intensity ($>$8–10 m s^{-1}) at all levels, including the apparent increase in downdraft intensity in the upper levels of the convective cell. The observation of strong downdraft cores aloft (possibly associated with the strongest updrafts) is consistent with Heymsfield et al. (2010), who report that their strongest downdraft observations occur above 10 km.

Few aircraft studies contained flights at very low levels that would possibly allow comparison with UAZR downdraft insights. In addition to the presence of strong updraft cores at low levels, UAZR datasets demonstrate that intense downdraft cores are possible at low altitudes. For this dataset, the largest downdraft diameters are typically observed at or below the melting layer and closer to the surface (consistent with near-surface downdraft divergence and evaporation). A majority of downdrafts and the most intense maximum downdrafts are also observed between the melting level and the surface. As discussed by May and Rajopadhyaya (1999), we anticipate the presence of these stronger downdraft cores as a consequence of precipitation loading and evaporation in stronger convective environments (with possible melting hail). The largest downdraft mass fluxes are therefore also observed closer to the surface. May and Rajopadhyaya (1999) further speculate that if the number of downdrafts can be assumed to remain relatively constant with height as with updrafts then it can be inferred that approximately two-thirds of the downdraft cores near or below the freezing level are buoyancy driven. Provided we make the same basic assumption, a similar finding (approximately one-half of the downdrafts being buoyantly driven) would be the case for our UAZR dataset.

It is not surprising that mass flux behavior for the continental UAZR dataset would not follow previous tropical (typically noncontinental) mass flux references. The UAZR 90th- and 95th-percentile mass flux estimates tend to be an order of magnitude greater than those reported in LZ and/or be comparable to the largest magnitudes recorded for the Amazon/Kwajalein Atoll studies of Anderson et al. (2005). Once again, these Oklahoma observations may still reflect the sampling of weaker cores relative to the strongest Heymsfield et al. (2010) observations and the possibly larger hail-producing storms of the Oklahoma region. Nevertheless, instantaneous maximum core mass flux values from the UAZR are even found to be 2–3 times those that were inferred in previous studies that included deeper continental convective elements (e.g., May and Rajopadhyaya 1999).

It is seen from the probability density function in Fig. 9 that the bulk of the observed mass flux is associated with cores of length smaller than 2 km and that only a small fraction of the observed mass flux is associated with larger-length cores. Negligible mass flux is attributed to very large cores of greater than 4–6 km, especially at the higher elevations (updrafts that were primarily observed above 6 km). Similar findings have been reported by LZ for tropical studies and have been echoed in the outputs of recent LES modeling studies (e.g., Khairoutdinov et al. 2009). It should be remembered that larger core sizes in the UAZR dataset are still those most often associated with larger individual core measurements of mass flux that are based on the present definition of mass flux in this study, which is calculated as the product of density, core length, and core velocity (Fig. 10).

6. Summary

A summary of deep convective updraft- and downdraft-core properties over the central plains of the United States demonstrates reasonable agreement with previous continental convective aircraft observations. This study was accomplished by using a novel but now standard ARM scanning mode for a commercial wind-profiler system. A unique profiler-based hydrometeor fall-speed correction method modeled for the convective environment was adopted. Accuracy of the velocity retrievals from this effort is expected to be within 1–2 m s^{-1} with minimal bias and a core-resolution capture of 1 km. Here, the authors refer to previous studies that attribute the relative behaviors of tropical to continental updraft profiles and core intensity to the differences in the magnitudes and vertical distributions of CAPE (e.g., Lucas et al. 1994), the possible role of hydrometeor unloading, and other factors (e.g., Heymsfield et al. 2010).

The key findings of this study are as follow:

1) Updraft cores are found in similar numbers with height, with an apparent increase in magnitude as a function of altitude to the mid- to upper storm levels. This profile behavior continues to the top of the usable UAZR storm data (~10–12 km). Profile behavior agrees well with previous Thunderstorm Project aircraft findings and the aircraft radar–based maximum velocity profile findings of Heymsfield et al. (2010). Intense cores with magnitudes exceeding 15 m s^{-1} are routinely observed, as was the case with the Heymsfield et al. (2010) findings.
2) Downdraft cores are found in lower numbers, and they are more frequently observed below the ambient freezing level. Downdraft magnitudes are found to be weaker than those of updrafts; substantial core

magnitudes are observed, however, with downdrafts exceeding $10\,m\,s^{-1}$.

3) The magnitudes of individual core mass fluxes are varied, yet observations are shown to be as high as an order of magnitude greater than aircraft values (calculated by similar means) that have been reported for tropical convection and/or to be comparable to the largest magnitudes recorded for Amazon/Kwajalein Atoll studies.
4) The majority of the observed mass flux for this dataset was associated with core lengths that were smaller than 2 km. Nearly 80% of the mass flux attributed to individual cores from these observations is associated with cores that were smaller than 4–6 km.
5) Weak, positive correlations are found between updraft intensity (maximum) and updraft length (r to 0.5 aloft). Negligible correlations are observed for downdraft core lengths and intensity.

Acknowledgments. This manuscript has been authored by employees of Brookhaven Science Associates, LLC, under Contract DE-AC02-98CH10886 with the U.S. Department of Energy. The publisher by accepting the manuscript for publication acknowledges that the U.S. government retains a nonexclusive, paid-up, irrevocable, worldwide license to publish or reproduce the published form of this manuscript, or to allow others to do so, for U.S. government purposes. Argonne National Laboratory's (ANL) work was supported by the Department of Energy, Office of Science, Office of Biological and Environmental Research (BER), under Contract DE-AC02-06CH11357. This research was also supported by the Office of Science (BER) of the Department of Energy under Grant DE-FG02-08ER64553. The research was also supported under Grant DE-SC0007080. Additional support was provided by the National Science Foundation under AGS-1036237 (Dr. Chungu Lu, program manager). In addition, the authors thank Pavlos Kollias, Michael Jensen, and ARM mentor Richard Coulter for their leadership roles with respect to the associated ARM Profiler and MC3E IOP campaign configurations and dataset collection. We also thank Edwin Campos of ANL for an internal review of this manuscript and Zac Flamig (OU/NSSL) for access to NSSL NEXRAD NMQ dataset archives.

REFERENCES

Ackerman, T. P., and G. M. Stokes, 2003: The Atmospheric Radiation Measurement Program. *Phys. Today,* **56,** 38–44.

Anderson, N. F., C. A. Grainger, and J. L. Stith, 2005: Characteristics of strong updrafts in precipitation systems over the central tropical Pacific Ocean and in the Amazon. *J. Appl. Meteor.,* **44,** 731–738.

Arakawa, A., and W. H. Schubert, 1974: Interaction of a cumulus cloud ensemble with the large-scale environment, Part I. *J. Atmos. Sci.,* **31,** 674–701.

Battan, L. J., and J. B. Theiss, 1970: Measurement of vertical velocities in convective clouds by means of pulsed-Doppler radar. *J. Atmos. Sci.,* **27,** 293–298.

Brandes, E. A., J. Vivekanandan, J. D. Tuttle, and C. J. Kessinger, 1995: A study of thunderstorm microphysics with multiparameter radar and aircraft observations. *Mon. Wea. Rev.,* **123,** 3129–3143.

Byers, H. R., and R. R. Braham, 1949: *The Thunderstorm—Report of the Thunderstorm Project.* U.S. Weather Bureau, 287 pp.

Campos, E. F., F. Fabry, and W. Hocking, 2007: Precipitation measurements using VHF wind profiler radars: Measuring rainfall and vertical air velocities using only observations with a VHF radar. *Radio Sci.,* **42,** RS3003, doi:10.1029/2006RS003540.

Cifelli, R., and S. Rutledge, 1994: Vertical motion structure in Maritime Continent mesoscale convective systems: Results from a 50-MHz profiler. *J. Atmos. Sci.,* **51,** 2631–2652.

Cronce, M., R. M. Rauber, K. R. Knupp, B. F. Jewett, J. T. Walters, and D. Phillips, 2007: Vertical motions in precipitation bands in three winter cyclones. *J. Appl. Meteor. Climatol.,* **46,** 1523–1543.

Del Genio, A. D., 2012: Representing the sensitivity of convective cloud systems to tropospheric humidity in general circulation models. *Surv. Geophys.,* **33,** 637–656.

——, W. Kovari, M.-S. Yao, and J. Jonas, 2005: Cumulus microphysics and climate sensitivity. *J. Climate,* **18,** 2376–2387.

——, J. Wu, and Y. Chen, 2012: Characteristics of mesoscale organization in WRF simulations of convection during TWP-ICE. *J. Climate,* **25,** 5666–5688.

Donner, L. J., 1993: A cumulus parameterization including mass fluxes, vertical momentum dynamics, and mesoscale effects. *J. Atmos. Sci.,* **50,** 889–906.

——, C. J. Seman, R. S. Hemler, and S. Fan, 2001: A cumulus parameterization including mass fluxes, convective vertical velocities, and mesoscale effects: Thermodynamic and hydrological aspects in a general circulation model. *J. Climate,* **14,** 3444–3463.

Ecklund, W. L., C. R. Williams, P. E. Johnston, and K. S. Gage, 1999: A 3-GHz profiler for precipitating cloud studies. *J. Atmos. Oceanic Technol.,* **16,** 309–322.

Ferrier, B. S., 1994: A two-moment multiple-phase four-class bulk ice scheme. Part I: Description. *J. Atmos. Sci.,* **51,** 249–280.

Foote, G. B., and P. S. Du Toit, 1969: Terminal velocity of raindrops aloft. *J. Appl. Meteor.,* **8,** 249–253.

Gal-Chen, T., 1982: Errors in fixed and moving frame of references: Applications for conventional and Doppler radar analysis. *J. Atmos. Sci.,* **39,** 2279–2300.

Geerts, B., and Y. Dawei, 2004: Classification and characterization of tropical precipitation based on high-resolution airborne vertical incidence radar. Part I: Classification. *J. Appl. Meteor.,* **43,** 1554–1566.

Gunn, R., and G. D. Kinzer, 1949: The terminal velocity of fall for water droplets in stagnant air. *J. Meteor.,* **6,** 243–248.

Heymsfield, G. M., L. Tian, A. J. Heymsfield, L. Li, and S. Guimond, 2010: Characteristics of deep tropical and subtropical convection from nadir-viewing high-altitude airborne Doppler radar. *J. Atmos. Sci.,* **67,** 285–308.

Igau, R. C., M. A. LeMone, and D. Wei, 1999: Updraft and downdraft cores in TOGA COARE: Why so many buoyant downdraft cores? *J. Atmos. Sci.,* **56,** 2232–2245.

Jakob, C., 2010: Accelerating progress in global atmospheric model development through improved parameterizations: Challenges, opportunities, and strategies. *Bull. Amer. Meteor. Soc.,* **91,** 869–875.

Jorgensen, D. P., E. J. Zipser, and M. A. LeMone, 1985: Vertical motions in intense hurricanes. *J. Atmos. Sci.,* **42,** 839–856.

Joss, J., and A. Waldvogel, 1967: A raindrop spectrograph with automatic analysis. *Pure Appl. Geophys.,* **68,** 240–246.

Khairoutdinov, M. F., S. K. Krueger, C.-H. Moeng, P. A. Bogenschutz, and D. A. Randall, 2009: Large-eddy simulation of maritime deep tropical convection. *J. Adv. Model. Earth Syst.,* **1,** 15, doi:10.3894/JAMES.2009.1.15.

Kyle, T. G., W. R. Sand, and D. J. Musil, 1976: Fitting measurements of thunderstorm updraft profiles to model profiles. *Mon. Wea. Rev.,* **104,** 611–617.

Laroche, S., and I. Zawadzki, 1994: A variational analysis method for retrieval of three-dimensional wind field from single-Doppler radar data. *J. Atmos. Sci.,* **51,** 2664–2682.

Lehmiller, G. S., H. B. Bluestein, P. J. Neiman, F. M. Ralph, and W. F. Feltz, 2001: Wind structure in a supercell thunderstorm as measured by a UHF wind profiler. *Mon. Wea. Rev.,* **129,** 1968–1986.

LeMone, M. A., and E. J. Zipser, 1980: Cumulonimbus vertical velocity events in GATE. Part I: Diameter, intensity and mass flux. *J. Atmos. Sci.,* **37,** 2444–2457.

Lenschow, D. H., 1976: Estimating updraft velocity from an airplane response. *Mon. Wea. Rev.,* **104,** 618–627.

Lerach, D. G., S. A. Rutledge, C. R. Williams, and R. Cifelli, 2010: Vertical structure of convective systems during NAME 2004. *Mon. Wea. Rev.,* **138,** 1695–1714.

Loney, M. L., D. S. Zrnić, J. M. Straka, and A. V. Ryzhkov, 2002: Enhanced polarimetric radar signatures above the melting level in a supercell storm. *J. Appl. Meteor.,* **41,** 1179–1194.

Lucas, C., E. J. Zipser, and M. A. LeMone, 1994: Vertical velocity in oceanic convection off tropical Australia. *J. Atmos. Sci.,* **51,** 3183–3193.

Marwitz, J. D., 1973: Trajectories within the weak echo regions of hailstorms. *J. Appl. Meteor.,* **12,** 1174–1182.

May, P. T., and R. G. Strauch, 1989: An examination of wind profiler signal processing algorithms. *J. Atmos. Oceanic Technol.,* **6,** 731–735.

——, and D. K. Rajopadhyaya, 1996: Wind profiler observations of vertical motion and precipitation microphysics of a tropical squall line. *Mon. Wea. Rev.,* **124,** 621–633; Corrigendum, **125,** 410–413.

——, and ——, 1999: Vertical velocity characteristics of deep convection over Darwin, Australia. *Mon. Wea. Rev.,* **127,** 1056–1071.

——, A. R. Jameson, T. D. Keenan, P. E. Johnston, and C. Lucas, 2002: Combined wind profiler/polarimetric radar studies of the vertical motion and microphysical characteristics of tropical sea breeze thunderstorms. *Mon. Wea. Rev.,* **130,** 2228–2239.

McLaughlin, D., and Coauthors, 2009: Short-wavelength technology and the potential for distributed networks of small radar systems. *Bull. Amer. Meteor. Soc.,* **90,** 1797–1817.

Milbrandt, J. A., and M. K. Yau, 2005: A multimoment bulk microphysics parameterization. Part I: Analysis of the role of the spectral shape parameter. *J. Atmos. Sci.,* **62,** 3051–3064.

Miller, L. J., J. D. Tuttle, and G. B. Foote, 1990: Precipitation production in a large Montana hailstorm: Airflow and particle growth trajectories. *J. Atmos. Sci.,* **47,** 1619–1646.

Musil, D. J., A. J. Heymsfield, and P. L. Smith, 1986: Microphysical characteristics of a well-developed weak echo region in a high plains supercell thunderstorm. *J. Climate Appl. Meteor.,* **25,** 1037–1051.

Protat, A., and I. Zawadzki, 1999: A variational method for real-time retrieval of three-dimensional wind field from multiple-Doppler bistatic radar network data. *J. Atmos. Oceanic Technol.,* **16,** 432–449.

——, and C. R. Williams, 2011: The accuracy of radar estimates of ice terminal fall speed from vertically pointing Doppler radar measurements. *J. Appl. Meteor. Climatol.,* **50,** 2120–2138.

Ray, P. S., C. L. Ziegler, W. Bumgarner, and R. J. Serafin, 1980: Single- and multiple-Doppler radar observations of tornadic storms. *Mon. Wea. Rev.,* **108,** 1607–1625.

Rosenfeld, D., W. L. Woodley, T. W. Krauss, and V. Makitov, 2006: Aircraft microphysical documentation from cloud base to anvils of hailstorm feeder clouds in Argentina. *J. Appl. Meteor. Climatol.,* **45,** 1261–1281.

Sand, W. R., 1976: Observations in hailstorms using the T-28 aircraft system. *J. Appl. Meteor.,* **15,** 641–650.

Sheppard, B. E., and P. I. Joe, 1994: Comparison of raindrop size distribution measurements by a Joss–Waldvogel disdrometer, a PMS 2DG spectrometer, and a POSS Doppler radar. *J. Atmos. Oceanic Technol.,* **11,** 874–887.

Shupe, M. D., P. Kollias, M. Poellot, and E. Eloranta, 2008: On deriving vertical air motions from cloud radar Doppler spectra. *J. Atmos. Oceanic Technol.,* **25,** 547–557.

Smith, P. L., D. J. Musil, A. G. Detwiler, and R. Ramachandran, 1999: Observations of mixed-phase precipitation within a CaPE thunderstorm. *J. Appl. Meteor.,* **38,** 145–155.

Steiner, M., 1991: A new relationship between mean Doppler velocity and differential reflectivity. *J. Atmos. Oceanic Technol.,* **8,** 430–443.

——, R. A. Houze Jr., and S. E. Yuter, 1995: Climatological characterization of three-dimensional storm structure from operational radar and rain gauge data. *J. Appl. Meteor.,* **34,** 1978–2007.

Stensrud, D. J., and Coauthors, 2009: Convective-scale warn-on-forecast system. *Bull. Amer. Meteor. Soc.,* **90,** 1487–1499.

Straka, J. M., and E. R. Mansell, 2005: A bulk microphysics parameterization with multiple ice precipitation categories. *J. Appl. Meteor.,* **44,** 445–466.

——, D. S. Zrnić, and A. V. Ryzhkov, 2000: Bulk hydrometeor classification and quantification using polarimetric radar data: Synthesis of relations. *J. Appl. Meteor.,* **39,** 1341–1372.

Tridon, F., A. Battaglia, P. Kollias, E. Luke and C. R. Williams, 2013: Signal postprocessing and reflectivity calibration of the Atmospheric Radiation Measurement 915-MHz wind profilers. *J. Atmos. Oceanic Technol.,* **30,** 1038–1054.

Uma, K. N., and T. N. Rao, 2009: Characteristics of vertical velocity cores in different convective systems observed over Gadanki, India. *Mon. Wea. Rev.,* **137,** 954–975.

Weisman, M. L., and J. B. Klemp, 1982: The dependence of numerically simulated convective storms on vertical wind shear and buoyancy. *Mon. Wea. Rev.,* **110,** 504–520.

Williams, C. R., 2012: Vertical air motion retrieved from dual-frequency profiler observations. *J. Atmos. Oceanic Technol.,* **29,** 1471–1480.

——, W. L. Ecklund, and K. S. Gage, 1995: Classification of precipitating clouds in the tropics using 915-MHz wind profilers. *J. Atmos. Oceanic Technol.,* **12,** 996–1012.

Yuter, S. E., and R. A. Houze Jr., 1995: Three-dimensional kinematic and microphysical evolution of Florida cumulonimbus. Part I: Spatial distribution of updrafts, downdrafts, and precipitation. *Mon. Wea. Rev.,* **123,** 1921–1940.

Zhang, S., K. Howard, and J. J. Gourley, 2005: Constructing three-dimensional multiple radar reflectivity mosaics: Examples of convective storms and stratiform rain echoes. *J. Atmos. Oceanic Technol.,* **22,** 30–42.